

Core-Level X-Ray Spectroscopy of Infinite-Layer Nickelate: LDA+DMFT Study

Keisuke Higashi,¹ Mathias Winder,² Jan Kuneš,² and Atsushi Hariki¹

¹*Department of Physics and Electronics, Graduate School of Engineering, Osaka Prefecture University 1-1 Gakuen-cho, Nakaku, Sakai, Osaka 599-8531, Japan*

²*Institute for Solid State Physics, TU Wien, 1040 Vienna, Austria*

(Dated: October 26, 2021)

Motivated by recent core-level x-ray photoemission spectroscopy, x-ray absorption spectroscopy (XAS), and resonant inelastic x-ray scattering (RIXS) experiments for the newly discovered superconducting infinite-layer nickelate, we investigate the core-level spectra of the parent compounds NdNiO₂ and LaNiO₂ using the combination of local density approximation and dynamical mean-field theory (LDA+DMFT). Adjusting a charge-transfer energy to match the experimental spectra, we determine the optimal model parameters and discuss the nature of the NdNiO₂ ground state. We find that self-doping from the Nd 5*d* states in the vicinity of the Fermi energy prohibits opening of a Mott-Hubbard gap in NdNiO₂. The present Ni *L*₃ XAS and RIXS calculation for LaNiO₂ cannot explain the difference from NdNiO₂ spectra.

I. INTRODUCTION

High-*T*_c superconductivity of cuprates has been a focal point of 3*d* transition-metal oxide (TMO) physics over the past 30 years [1–3]; nevertheless, the underlying mechanism remains elusive. Superconductivity [4] reported recently in layered nickelate Nd_{0.8}Sr_{0.2}NiO₂ (*T*_c = 9–15 K) with a similar crystal structure may provide new clues. The fundamental question is whether the electronic structure of NdNiO₂ (and LaNiO₂) is similar to that of high-*T*_c cuprates. Naively, one might presume that Ni in the undoped systems is monovalent and, thus, hosts the *d*⁹ (*S* = 1/2) ground state similar to cuprates. However, theoretical studies [5–9] suggest a self-doping from Nd (or La) 5*d* orbitals. Additionally, holes doped to a low-valence Ni¹⁺ compound may reside in Ni 3*d* orbitals, unlike in cuprates [2, 3, 10] or NiO with Ni²⁺ [11], where they occupy the O 2*p* states.

The Ni 2*p*_{3/2} core-level x-ray photoemission spectroscopy (XPS) [12], x-ray absorption spectroscopy (XAS), and resonant inelastic x-ray scattering (RIXS) [9, 13] are employed to probe the electronic structure of infinite-layer nickelates. A shoulder observed in the main line of the Ni 2*p*_{3/2} XPS spectra in NdNiO₂ [12] is attributed to Ni-Ni charge-transfer (CT) response to the creation of the core hole, a process traditionally called nonlocal screening (NLS) [14]. Generally, NLS provides valuable information about the electronic structure of TMOs [15–18]. For high-*T*_c cuprates, the NLS in Cu 2*p*_{3/2} XPS is extensively used to determine key parameters, such as the CT energy Δ_{dp} , and more recently to analyze electronic reconstructions due to doping [19–23].

Further information can be obtained with charge-conserving spectroscopies XAS and RIXS. The Ni *L*₃-edge XAS and RIXS spectra are measured in both NdNiO₂ [9, 13] and LaNiO₂ [9]. Interestingly, a side peak (852.0 eV) is observed in *L*₃-XAS of LaNiO₂, while it is absent in NdNiO₂. A low-energy RIXS feature (*E*_{loss} = 0.6 eV) associated with the XAS side peak is observed in LaNiO₂. The difference between the Ni *L*₃ XAS

and RIXS spectra of NdNiO₂ and LaNiO₂ poses an open question.

In this paper, we use the local-density approximation (LDA) + dynamical mean-field theory (DMFT) [24–26] to calculate XPS, XAS, and RIXS spectra [16, 27–30] of undoped infinite-layer nickelates. By comparison with the available experimental data, we identify the most appropriate CT energy and use it for classification within the Zaanen-Sawatzky-Allen scheme [10].

Material-specific DMFT calculations for NdNiO₂ or LaNiO₂ were performed by several authors, leading to contradictory conclusions, which can be sorted into two groups: (i) Multiorbital (Hund’s metal) physics is crucial [31–34], and (ii) (single-orbital) Mott-Hubbard physics is relevant with little influence of charge-transfer effects or with a small self-doping by Nd 5*d* electrons [35–37]. The differences, recently addressed blueby Karp, Hampel, and Millis [38], can be traced to the model parameters, which are not uniquely defined, such as the interaction strength, orbital basis, and, in particular, the double-counting correction. To settle the debate, an experimental input is needed to provide a benchmark for selecting the model parameters.

II. COMPUTATIONAL METHOD

The XPS, XAS and RIXS simulations start with a standard LDA+DMFT calculation [16, 25–28, 39]. First, LDA bands for the experimental crystal structure of NdNiO₂ and LaNiO₂ [4, 40] are calculated using the Wien2K package [41][42] and projected onto Wannier basis spanning the Ni 3*d*, O 2*p*, and Nd (La) 5*d* orbitals [43, 44]. The model is augmented with a local electron-electron interaction within the Ni 3*d* shell, parametrized by Coulomb’s *U* = 5.0 eV and Hund’s *J* = 1.0 eV [31, 32, 45]. The strong-coupling continuous-time quantum Monte Carlo impurity solver [46–49] is employed with the DMFT cycle to obtain the Ni 3*d* self-energy $\Sigma(i\omega_n)$, which is analytically continued [50] to real frequency after having reached the self-consistency. The

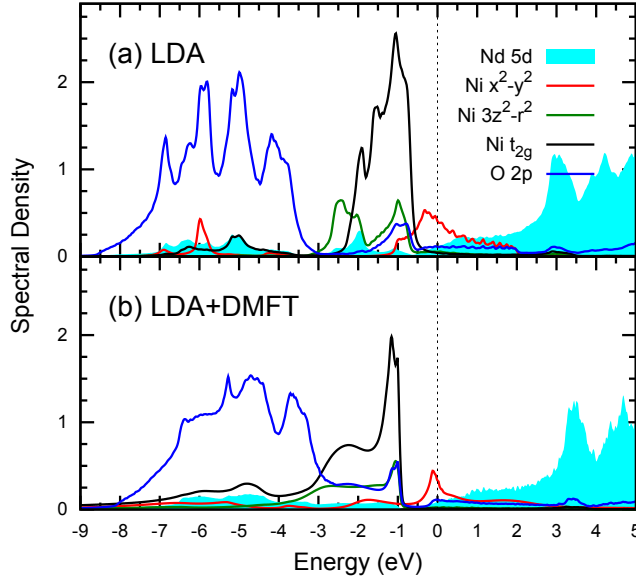


FIG. 1. The one-particle spectral densities of NdNiO₂ obtained by (a) LDA and (b) LDA+DMFT (for $\Delta_{dp} = 4.9$ eV).

calculations are performed at temperature $T = 290$ K.

The XPS, XAS, and RIXS spectra are calculated from the Anderson impurity model augmented with the $2p$ core states and the real-frequency hybridization function discretized into 40–50 levels (per spin and orbital). To this end, we use the configuration-interaction solver; for details, see Refs. 16 and 29 for XPS and Refs. 27, 28, and 51 for XAS and RIXS simulation.

Determination of Ni $3d$ site energies in the model studied by DMFT involves subtracting the so-called double-counting correction μ_{dc} from the respective LDA values ($\varepsilon_d^{\text{LDA}}$), a procedure accounting for the effect of the dd interaction present in the LDA description. It is clear that μ_{dc} is of the order of Hartree energy Un_d , but a generally accepted universal expression is not available [26, 52, 53]. While a similar uncertainty exists also for interaction parameters U and J , impact of their variation on physical properties is usually minor (see Supplemental Material [54] for NdNiO₂-specific discussion). Variation of μ_{dc} , on the other hand, may have a profound effect. Therefore we choose to adjust μ_{dc} by comparison to the experimental data. Although μ_{dc} is the parameter entering the calculation, in the discussion we use its linear function $\Delta_{dp} = (\varepsilon_d^{\text{LDA}} - \mu_{dc}) + 9U_{dd} - \varepsilon_p^{\text{LDA}}$, which sets the scale for the energy necessary to transfer an electron from O $2p$ to Ni $3d$ orbital. Here, $U_{dd} = U - \frac{4}{9}J$ is the average interorbital interaction, and 9 is the Ni $3d$ occupation in the Ni⁺ formal valence (similar to the definition of the charge-transfer energy in the cluster model [28, 29, 55]).

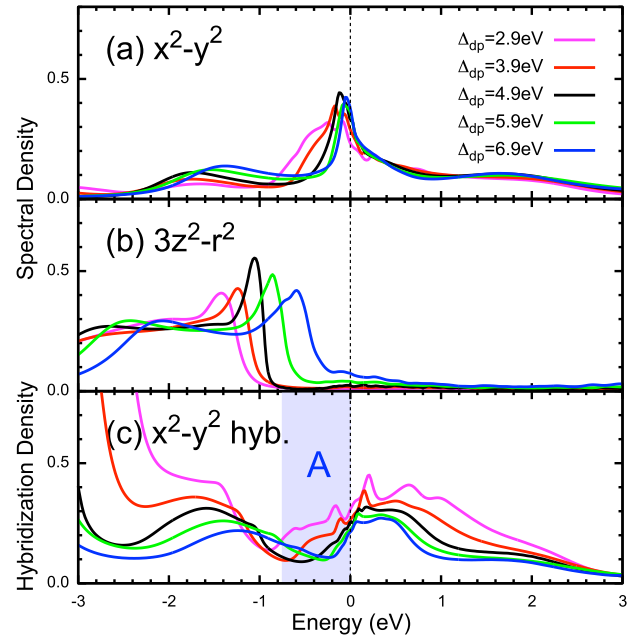


FIG. 2. The DMFT spectral densities for (a) Ni $x^2 - y^2$ and (b) Ni $3z^2 - r^2$ orbitals along with (c) the Ni $x^2 - y^2$ hybridization function computed for different Δ_{dp} values.

III. ELECTRONIC STRUCTURE

Figure 1 shows the orbitally resolved spectral densities (projected density of states) of NdNiO₂ obtained by LDA and LDA+DMFT for $\Delta_{dp} = 4.9$ eV, which we later identify as the optimal parameter choice. Both the LDA and LDA+DMFT yield a metallic state with the Ni $x^2 - y^2$ orbital character dominating around the Fermi level. This general picture is valid in the entire range of studied $\Delta_{dp} = 2.9 - 6.9$ eV. In Fig. 2, we show the dependence of Ni $x^2 - y^2$ and $3z^2 - r^2$ spectra on Δ_{dp} . Increasing Δ_{dp} corresponds to an upward shift of the bare Ni $3d$ site energies, which is indirectly reflected in the shift of the $3z^2 - r^2$ band. The $x^2 - y^2$ peak at the Fermi level, rather than being shifted, exhibits an increased mass renormalization (reduced width). The amplitude of the $x^2 - y^2$ hybridization function around the Fermi level is reduced with increasing Δ_{dp} ; in particular, the sizable decrease just below the Fermi level (blue region) has an important implication for the XPS spectra as discussed later. The evolution of $x^2 - y^2$ and $3z^2 - r^2$ occupancies in Fig. 4 shows that, up to $\Delta_{dp} \approx 7$ eV the $3z^2 - r^2$ is completely filled (the deviation from 2.0 is due to hybridization with empty bands). The physics is, thus, effectively of a single-orbital Hubbard model, and the Ni ion takes a monovalent (Ni¹⁺, d^9) character.

Different from cuprates, the stoichiometric parent compound is metallic. In order to analyze the role of Nd d bands, we study two modified models: (i) hybridization between NiO₂ planes and the Nd orbitals is switched off, and (ii) Nd orbitals are removed from the model. In the

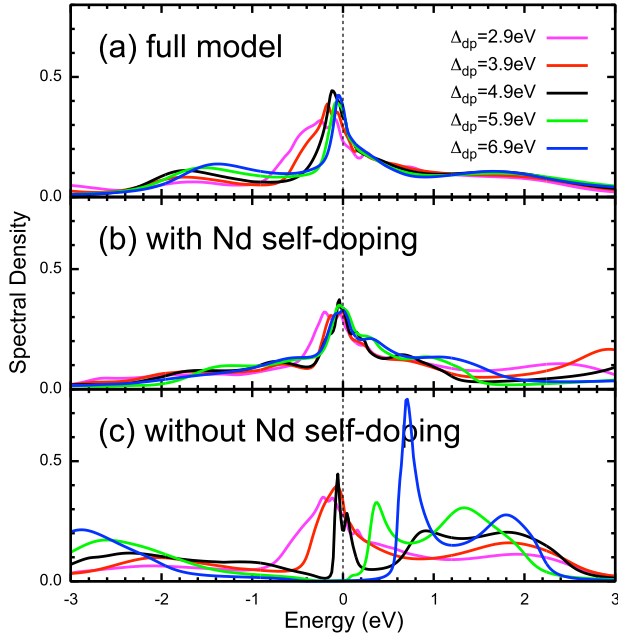


FIG. 3. The $x^2 - y^2$ spectral densities computed in (a) the full model [the same as in Fig. 2(a)], (b) model (i) with a self-doping from Nd d bands, and (c) model (ii) without a self-doping from Nd d bands.

former case (i) self-doping of the NiO_2 planes from Nd orbitals is possible, while in the latter case (ii) the stoichiometry of the NiO_2 planes cannot change. The evolution of the $x^2 - y^2$ spectral density with Δ_{dp} for (i) and (ii) is shown in Fig. 3. Like the full model, the low-energy spectrum of model (i) remains metallic over the whole studied range of Δ_{dp} . Removing the Nd orbitals (ii) results in progressive mass renormalization with increasing Δ_{dp} and eventually opening of a gap above $\Delta_{dp} = 5.9$ eV. This can be understood as a result of effective weakening of the Ni-O hybridization, i.e., a bandwidth-driven Mott transition. The NiO_2 layers in NdNiO_2 can, thus, be viewed as a strongly correlated system in the vicinity of Mott transition, where the insulating state is precluded by the presence of Nd $5d$ bands [56].

IV. COMPARISON TO EXPERIMENTAL X-RAY SPECTROSCOPIES

A. Ni $2p_{3/2}$ XPS

Next, we investigate the impact of the variation of Δ_{dp} on the core-level spectra. Figure 5 shows the calculated Ni $2p_{3/2}$ XPS spectra of NdNiO_2 together with the experimental data [12]. The Ni $2p_{3/2}$ XPS spectrum consists of two components: the main-line (852–857 eV) and the CT satellite (861 eV) [16, 55]. The core hole created by x rays represents an attractive potential, which induces CT from surrounding atoms to the empty $3d$ orbital on

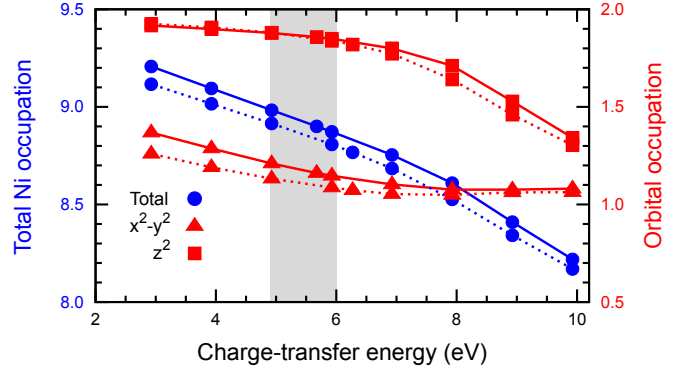


FIG. 4. The DMFT occupation of $x^2 - y^2$ (red, square) and $3z^2 - r^2$ (red, triangle) orbitals and the entire Ni $3d$ shell (blue, circle) as a function of Δ_{dp} . The full line is obtained for NdNiO_2 , and the dashed line for $\text{Nd}_{0.775}\text{Sr}_{0.225}\text{NiO}_2$.

the excited Ni site. The main line corresponds to the CT screened final states, while the CT satellite corresponds to unscreened ones [14, 16, 23]. Fu *et al.* [12] observe a shoulder B (approximately 856.5 eV) in the main line. Unlike A , the peak B is absent in the cluster-model spectra [14, 29] and, thus, can be ascribed to NLS [12]. The sensitivity of the relative intensity of A and B to Δ_{dp} can be used to locate its value to the interval 4.9–5.9 eV. The observed behavior of the NLS feature B reflects the amplitude of the hybridization function just below the Fermi level [16], the shaded area in Fig. 2(c).

The NLS (B) is known to dominate over the local screening (A) in cuprates, as shown in Fig. 5 for Cu $2p_{3/2}$ XPS in La_2CuO_4 [19]. For small $\Delta_{dp} = 2.9$ eV, a typical value for high- T_c cuprates [10, 14, 19, 23, 57], the spectra of NdNiO_2 resemble that of La_2CuO_4 . Thus our analysis shows that Δ_{dp} in NdNiO_2 is by 2–3 eV larger than in cuprates. The relative size Δ_{dp} and the Hubbard U would place NdNiO_2 somewhere between the Mott-Hubbard ($\Delta_{dp} > U$) and CT ($\Delta_{dp} < U$) systems in the Zaanen-Sawatzky-Allen classification of TMOs [10, 37, 58, 59]. The calculated occupations for doped $\text{Nd}_{0.775}\text{Sr}_{0.225}\text{NiO}_2$, shown in Fig. 4 and in Supplementary Material [54], reveal that for optimal Δ_{dp} doped holes are almost equally shared by Ni, Nd and O sites. This is a remarkable difference to monovalent cuprates or divalent NiO. In these systems of strong charge-transfer character, the doped holes reside predominantly in O $2p$ orbitals, irrespective of a substantial $3d$ spectral weight just below the Fermi level [60]. Moreover, for the optimal Δ_{dp} values inferred above, the doped holes in NdNiO_2 do not enter the Ni $3z^2 - r^2$ orbitals (Fig. 4). The single-band Hubbard description is thus valid for not only the parent NdNiO_2 but also the superconducting one $\text{Nd}_{0.8}\text{Sr}_{0.2}\text{NiO}_2$, as suggested by Refs. [35–37].

Proximity to NiO_2 layers to a Mott state (precluded by self-doping from Nd) suggests that a superexchange interaction still plays a role despite the metallic state. Using the optimal Δ_{dp} we arrive [54] at the nearest Ni–

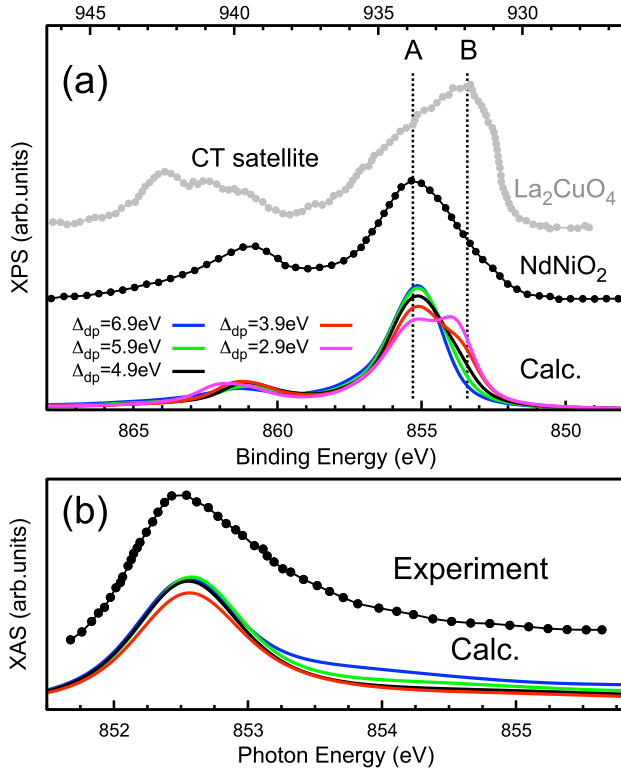


FIG. 5. (a) Ni $2p_{3/2}$ XPS spectra and (b) Ni $2p_{3/2}$ XAS spectra of NdNiO₂ calculated by the LDA+DMFT method for different Δ_{dp} values. The experimental data [9, 12] are shown together. For comparison, experimental Cu $2p_{3/2}$ XPS data of La₂CuO₄ are shown (gray) [19]. The spectral broadening is taken into account using a Lorentzian 300 meV (HWHM) and a Gaussian 250 meV (HWHM) for XAS and a Lorentzian 500 meV and a Gaussian 400 meV for XPS. The XPS spectra with different broadening widths can be found in Supplemental Material [54].

Ni anti-ferromagnetic exchange in the range 40–60 meV. Given the oversimplification of representing spin response of a metal in terms of local moments interactions, this value is consistent with 69 meV inferred from the RIXS experiment on a related compound La₄Ni₃O₈ [61]

The calculated LaNiO₂ spectra in Fig. 6(a) show similar behavior to NdNiO₂.

B. Ni $2p_{3/2}$ XAS and RIXS

As expected for Ni¹⁺ systems with a d^9 configuration, the experimental Ni $2p_{3/2}$ XAS of NdNiO₂ shows a sharp peak corresponding to the electron excitation from the $2p_{3/2}$ to an empty $x^2 - y^2$ orbital [Fig. 5(b)]. The XAS main peak is accompanied by a broad tail attributed to the hybridization with metallic bands. The theoretical results in Fig. 5(b) reproduce the experimental data reasonably well; however, the weak dependence on Δ_{dp} does not allow to draw conclusions about its value.

The RIXS spectra, on the other hand, exhibit fine

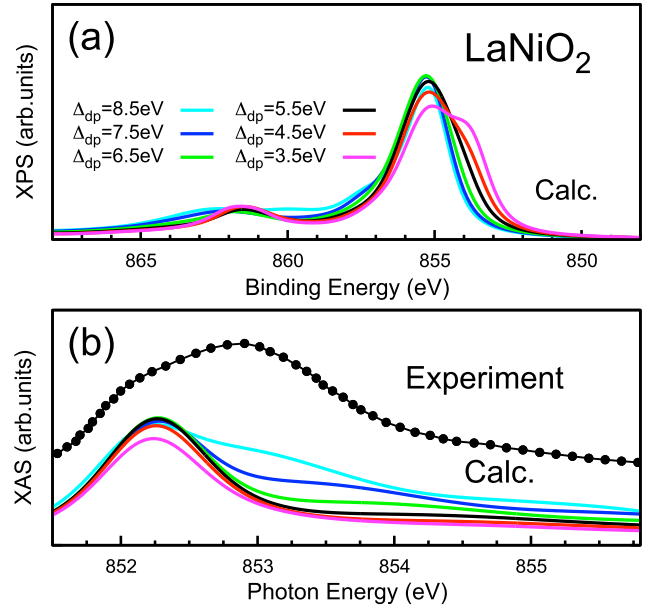


FIG. 6. (a) Ni $2p_{3/2}$ XPS spectra and (b) Ni $2p_{3/2}$ XAS spectra of LaNiO₂ calculated by the LDA+DMFT method for different Δ_{dp} values. The spectral broadening is taken into account using a Lorentzian 300 meV (HWHM) and a Gaussian 250 meV (HWHM) for XAS, and a Lorentzian 500 meV and a Gaussian 400 meV for XPS.

changes with the Δ_{dp} values, see Fig. 7. The spectra at all Δ_{dp} values contain a strong Raman-like (RL) feature (at constant E_{loss} irrespective of the incident photon energies E_{in}) at $E_{\text{loss}} \sim 1$ eV and a fluorescence-like (FL) feature (E_{loss} linearly increases with E_{in}). The RL feature arises from $t_{2g} \rightarrow x^2 - y^2$ excitation, and its width (in E_{loss}) reflects a rapid decay of this local "exciton". With increasing Δ_{dp} , the RL feature shifts to lower energies, due upward shift to the t_{2g} bands similar to $3z^2 - r^2$ shown in Fig. 2(b), while the $x^2 - y^2$ peaks remain pinned in the vicinity of the Fermi level. The main variation of the RIXS spectra with increasing Δ_{dp} concerns the behavior of the FL part, the onset of which is pushed to higher E_{loss} . For $\Delta_{dp}=4.9$ eV, deduced from the XPS data, the FL feature sets in below the RL feature at around $E_{\text{loss}} \sim 0.6$ eV. The coexisting RL and FL features above well capture the experimental data by Hepting *et al.* [9] and Rossi *et al.* [13]. Artificial suppression of hybridization to Nd $5d$ states [Fig. 7(e)] leads to a reduced intensity of the FL feature and only a moderate modification of the low-energy spectra supporting the conclusion about the electron-reservoir role of Nd $5d$ states.

Finally we discuss XAS and RIXS spectra in LaNiO₂ (the experimental XPS data are not available at the moment). The experimental XAS spectra of LaNiO₂ [9] are clearly distinct from NdNiO₂. A side peak at 852.0 eV is attributed to Ni–La hybridization effect by Hepting *et al.* [9] based on a simplified impurity model simulation. The LDA+DMFT calculations (including Ni–La hybridization) do not support this conclusion as they do

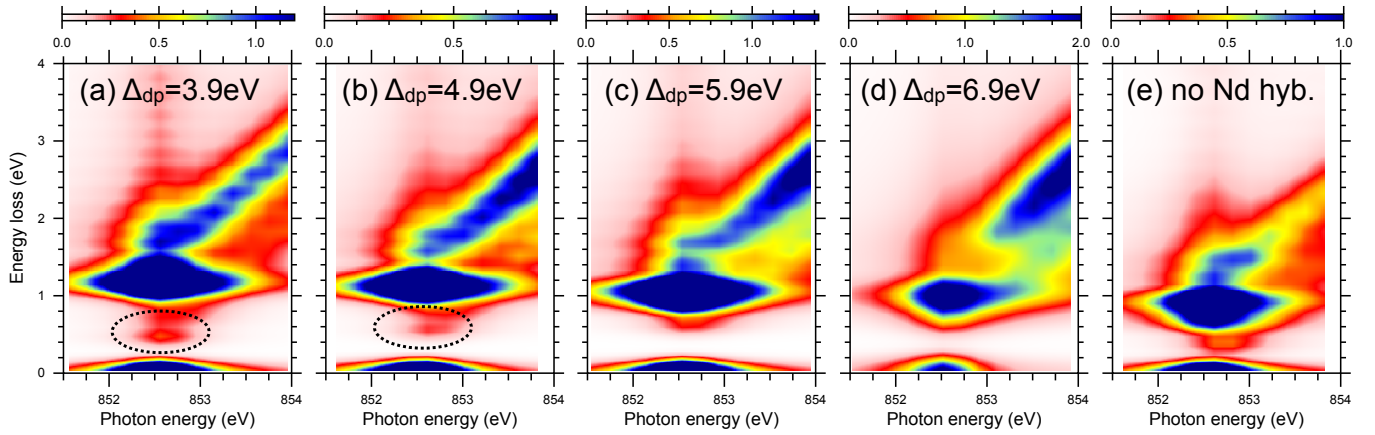


FIG. 7. The Ni L_3 RIXS spectra of NdNiO₂ calculated for (a) $\Delta_{dp} = 3.9$ eV, (b) $\Delta_{dp} = 4.9$ eV, (c) $\Delta_{dp} = 5.9$ eV, and (d) $\Delta_{dp} = 6.9$ eV. (e) the Ni L_3 RIXS spectra calculated for the model without the hybridization between Nd 5d and NiO₂ plane ($\Delta_{dp}=4.9$ eV). The spectral broadening is considered using a Gaussian of 100 meV (HWHM).

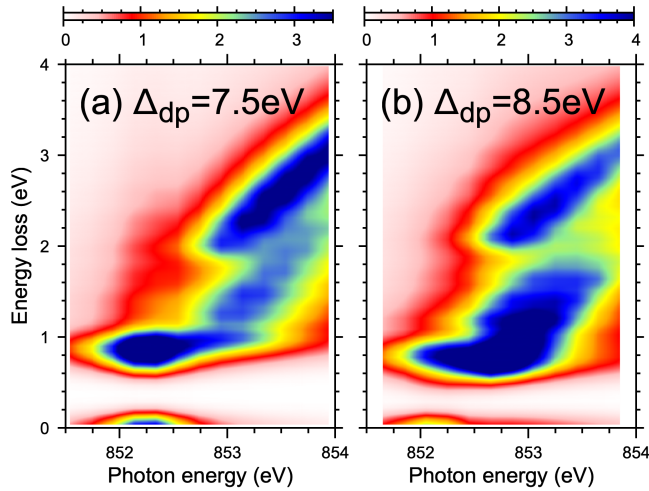


FIG. 8. The Ni L_3 RIXS spectra of LaNiO₂ calculated for (a) $\Delta_{dp} = 7.5$ eV, (b) $\Delta_{dp} = 8.5$ eV. The spectral broadening is considered using a Gaussian of 100 meV (HWHM).

not match the experimental XAS spectra. While large Δ_{dp} gives rise to a high-energy XAS shoulder (Fig. 6), it does not improve the agreement of the RIXS spectra, shown in Fig. 8. We have to conclude that the present LDA+DMFT description of LaNiO₂ does not match the experiment for any choice of Δ_{dp} .

We propose that the problem lies on the experimental side; i.e., the measured spectra do not represent a perfect LaNiO₂ crystal. We argue by the success of the present method for a broad spectrum of transition-metal oxides [16] including NdNiO₂ as well as the absence of an obvious source of difference between NdNiO₂ and LaNiO₂. On the experimental side, we point out recent studies [62, 63] reporting superconductivity in Sr-doped LaNiO₂, suggesting that NdNiO₂ and LaNiO₂ are not that different after all. Spectroscopic experiments

on these new LaNiO₂ samples are needed to resolve the present discrepancy.

V. CONCLUSIONS

We have presented a comprehensive analysis of Ni $2p_{3/2}$ core-level XPS, XAS, and RIXS in infinite-layer nickelates (NdNiO₂ and LaNiO₂) with the LDA+DMFT approach. Comparison to the experimental spectra allowed us to determine the CT parameter (double-counting correction) and make the following conclusions about the electronic structure. Undoped NdNiO₂ is nearly monovalent (Ni¹⁺, d^9) with a small self-doping from the Nd 5d band. Only the Ni $x^2 - y^2$ orbitals are partially filled and multiorbital physics does not play an important role for the stoichiometric as well as slightly hole-doped compound. Unlike in cuprates, the Ni-O hybridization does not play an important role in connection with doping – doped holes reside predominantly on the Ni sites. The physics of NdNiO₂ described effectively by a single-band Hubbard model [35–37] is consistent with the available core-level spectroscopies. While the present calculations provide a good description of the experimental core-level spectra of NdNiO₂, we cannot explain the qualitative difference between the reported NdNiO₂ and LaNiO₂ XAS and RIXS spectra.

ACKNOWLEDGMENTS

We thank M. Kitatani, K. Yamagami, T. Uozumi, H. Ikeno, L. Si, M.-J. Huang and R.-P. Wang for valued discussions. A.H., M.W., and J.K. were supported by the European Research Council (ERC) under the European Union’s Horizon 2020 research and innovation program (Grant Agreement No. 646807-EXMAG). A.H. was supported by JSPS KAKENHI Grant No. 21K13884. The

numerical calculations were performed at the Vienna Scientific Cluster (VSC).

-
- [1] J. G. Bednorz and K. A. Müller, *Z. Phys., B Condens. matter* **64**, 189 (1986).
- [2] M. Imada, A. Fujimori, and Y. Tokura, *Rev. Mod. Phys.* **70**, 1039 (1998).
- [3] E. Dagotto, *Rev. Mod. Phys.* **66**, 763 (1994).
- [4] D. Li, K. Lee, B. Y. Wang, M. Osada, S. Crossley, H. R. Lee, Y. Cui, Y. Hikita, and H. Y. Hwang, *Nature* **572**, 624 (2019).
- [5] A. S. Botana and M. R. Norman, *Phys. Rev. X* **10**, 011024 (2020).
- [6] J. Krishna, H. LaBollita, A. O. Fumega, V. Pardo, and A. S. Botana, *Phys. Rev. B* **102**, 224506 (2020).
- [7] K.-W. Lee and W. E. Pickett, *Phys. Rev. B* **70**, 165109 (2004).
- [8] G.-M. Zhang, Y.-f. Yang, and F.-C. Zhang, *Phys. Rev. B* **101**, 020501 (2020).
- [9] M. Hepting, D. Li, C. J. Jia, H. Lu, E. Paris, Y. Tseng, X. Feng, M. Osada, E. Been, Y. Hikita, Y.-D. Chuang, Z. Hussain, K. J. Zhou, A. Nag, M. Garcia-Fernandez, M. Rossi, H. Y. Huang, D. J. Huang, Z. X. Shen, T. Schmitt, H. Y. Hwang, B. Moritz, J. Zaanen, T. P. Devereaux, and W. S. Lee, *Nat. Mater.* **19**, 381 (2020).
- [10] J. Zaanen, G. A. Sawatzky, and J. W. Allen, *Phys. Rev. Lett.* **55**, 418 (1985).
- [11] J. Kuneš, V. I. Anisimov, S. L. Skornyakov, A. V. Lukoyanov, and D. Vollhardt, *Phys. Rev. Lett.* **99**, 156404 (2007).
- [12] Y. Fu, L. Wang, H. Cheng, S. Pei, X. Zhou, J. Chen, S. Wang, R. Zhao, W. Jiang, C. Liu, M. Huang, X. Wang, Y. Zhao, D. Yu, F. Ye, S. Wang, and J.-W. Mei, (2019), arXiv:1911.03177.
- [13] M. Rossi, H. Lu, A. Nag, D. Li, M. Osada, K. Lee, B. Y. Wang, S. Agrestini, M. Garcia-Fernandez, Y. D. Chuang, Z. X. Shen, H. Y. Hwang, B. Moritz, K.-J. Zhou, T. P. Devereaux, and W. S. Lee, (2020), arXiv:2011.00595.
- [14] M. A. van Veenendaal and G. A. Sawatzky, *Phys. Rev. Lett.* **70**, 2459 (1993).
- [15] M. van Veenendaal, *Phys. Rev. B* **74**, 085118 (2006).
- [16] A. Hariki, T. Uozumi, and J. Kuneš, *Phys. Rev. B* **96**, 045111 (2017).
- [17] M. Taguchi and G. Panaccione, “Depth-dependence of electron screening, charge carriers and correlation: Theory and experiments,” in *Hard X-ray Photoelectron Spectroscopy (HAXPES)*, edited by J. C. Woicik (Springer International Publishing, Cham, 2016) pp. 197–216.
- [18] M. Taguchi, M. Matsunami, Y. Ishida, R. Eguchi, A. Chainani, Y. Takata, M. Yabashi, K. Tamasaku, Y. Nishino, T. Ishikawa, Y. Senba, H. Ohashi, and S. Shin, *Phys. Rev. Lett.* **100**, 206401 (2008).
- [19] M. Taguchi, A. Chainani, K. Horiba, Y. Takata, M. Yabashi, K. Tamasaku, Y. Nishino, D. Miwa, T. Ishikawa, T. Takeuchi, K. Yamamoto, M. Matsunami, S. Shin, T. Yokoya, E. Ikenaga, K. Kobayashi, T. Mochiku, K. Hirata, J. Hori, K. Ishii, F. Nakamura, and T. Suzuki, *Phys. Rev. Lett.* **95**, 177002 (2005).
- [20] M. Horio, Y. Krockenberger, K. Yamamoto, Y. Yokoyama, K. Takubo, Y. Hirata, S. Sakamoto, K. Koshiishi, A. Yasui, E. Ikenaga, S. Shin, H. Yamamoto, H. Wadati, and A. Fujimori, *Phys. Rev. Lett.* **120**, 257001 (2018).
- [21] K. Okada and A. Kotani, *Phys. Rev. B* **52**, 4794 (1995).
- [22] M. A. van Veenendaal, G. A. Sawatzky, and W. A. Groen, *Phys. Rev. B* **49**, 1407 (1994).
- [23] M. Taguchi, A. Chainani, N. Kamakura, K. Horiba, Y. Takata, M. Yabashi, K. Tamasaku, Y. Nishino, D. Miwa, T. Ishikawa, S. Shin, E. Ikenaga, T. Yokoya, K. Kobayashi, T. Mochiku, K. Hirata, and K. Motoya, *Phys. Rev. B* **71**, 155102 (2005).
- [24] W. Metzner and D. Vollhardt, *Phys. Rev. Lett.* **62**, 324 (1989).
- [25] A. Georges, G. Kotliar, W. Krauth, and M. J. Rozenberg, *Rev. Mod. Phys.* **68**, 13 (1996).
- [26] G. Kotliar, S. Y. Savrasov, K. Haule, V. S. Oudovenko, O. Parcollet, and C. A. Marianetti, *Rev. Mod. Phys.* **78**, 865 (2006).
- [27] A. Hariki, M. Winder, and J. Kuneš, *Phys. Rev. Lett.* **121**, 126403 (2018).
- [28] A. Hariki, M. Winder, T. Uozumi, and J. Kuneš, *Phys. Rev. B* **101**, 115130 (2020).
- [29] M. Ghiasi, A. Hariki, M. Winder, J. Kuneš, A. Regoutz, T.-L. Lee, Y. Hu, J.-P. Rueff, and F. M. F. de Groot, *Phys. Rev. B* **100**, 075146 (2019).
- [30] J. Kolorenč, *Physica B Condens. Matter.* **536**, 695 (2018).
- [31] Y. Wang, C.-J. Kang, H. Miao, and G. Kotliar, *Phys. Rev. B* **102**, 161118 (2020).
- [32] C.-J. Kang and G. Kotliar, *Phys. Rev. Lett.* **126**, 127401 (2021).
- [33] F. Petocchi, V. Christiansson, F. Nilsson, F. Aryasetiawan, and P. Werner, *Phys. Rev. X* **10**, 041047 (2020).
- [34] F. Lechermann, *Phys. Rev. X* **10**, 041002 (2020).
- [35] J. Karp, A. S. Botana, M. R. Norman, H. Park, M. Zingl, and A. Millis, *Phys. Rev. X* **10**, 021061 (2020).
- [36] M. Kitatani, L. Si, O. Janson, R. Arita, Z. Zhong, and K. Held, *npj Quantum Materials* **5**, 59 (2020).
- [37] J. Karp, A. Hampel, M. Zingl, A. S. Botana, H. Park, M. R. Norman, and A. J. Millis, *Phys. Rev. B* **102**, 245130 (2020).
- [38] J. Karp, A. Hampel, and A. J. Millis, (2021), arXiv:2102.08522.
- [39] J. Kuneš, I. Leonov, M. Kollar, K. Byczuk, V. I. Anisimov, and D. Vollhardt, *Eur. Phys. J. Spec. Top.* **180**, 5 (2009).
- [40] M. A. Hayward, M. A. Green, M. J. Rosseinsky, and J. Sloan, *Journal of the American Chemical Society* **121**, 8843 (1999), <https://doi.org/10.1021/ja991573i>.
- [41] P. Blaha, K. Schwarz, G. Madsen, D. Kvasnicka, and J. Luitz, *WIEN2k, An Augmented Plane Wave + Local Orbitals Program for Calculating Crystal Properties* (Karlheinz Schwarz, Techn. Universität Wien, Austria, 2001, ISBN 3-9501031-1-2).
- [42] The Nd 4f states in NdNiO₂ are treated as partially-filled core states.
- [43] J. Kuneš, R. Arita, P. Wissgott, A. Toschi, H. Ikeda, and K. Held, *Comput. Phys. Commun.* **181**, 1888 (2010).

- [44] A. A. Mostofi, J. R. Yates, G. Pizzi, Y.-S. Lee, I. Souza, D. Vanderbilt, and N. Marzari, *Comput. Phys. Commun.* **185**, 2309 (2014).
- [45] S. Ryee, H. Yoon, T. J. Kim, M. Y. Jeong, and M. J. Han, *Phys. Rev. B* **101**, 064513 (2020).
- [46] P. Werner, A. Comanac, L. de' Medici, M. Troyer, and A. J. Millis, *Phys. Rev. Lett.* **97**, 076405 (2006).
- [47] L. Boehnke, H. Hafermann, M. Ferrero, F. Lechermann, and O. Parcollet, *Phys. Rev. B* **84**, 075145 (2011).
- [48] H. Hafermann, K. R. Patton, and P. Werner, *Phys. Rev. B* **85**, 205106 (2012).
- [49] A. Hariki, A. Yamanaka, and T. Uozumi, *J. Phys. Soc. Jpn.* **84**, 073706 (2015).
- [50] M. Jarrell and J. Gubernatis, *Phys. Rep.* **269**, 133 (1996).
- [51] M. Winder, A. Hariki, and J. Kuneš, *Phys. Rev. B* **102**, 085155 (2020).
- [52] M. Karolak, G. Ulm, T. Wehling, V. Mazurenko, A. Poteryaev, and A. Lichtenstein, *J. Electron. Spectrosc. Relat. Phenom.* **181**, 11 (2010).
- [53] K. Haule, *Phys. Rev. Lett.* **115**, 196403 (2015).
- [54] See Supplementary Material for model-parameter dependence of Ni density of states, hybridization intensity, and Ni 2p XPS spectra.
- [55] F. de Groot and A. Kotani, *Core Level Spectroscopy of Solids* (CRC Press, Boca Raton, FL, 2014).
- [56] M. Hirayama, T. Tadano, Y. Nomura, and R. Arita, *Phys. Rev. B* **101**, 075107 (2020).
- [57] J. Ghijsen, L. H. Tjeng, J. van Elp, H. Eskes, J. Westering, G. A. Sawatzky, and M. T. Czyzyk, *Phys. Rev. B* **38**, 11322 (1988).
- [58] Y. Nomura, T. Nomoto, M. Hirayama, and R. Arita, *Phys. Rev. Research* **2**, 043144 (2020).
- [59] Y. Nomura, M. Hirayama, T. Tadano, Y. Yoshimoto, K. Nakamura, and R. Arita, *Phys. Rev. B* **100**, 205138 (2019).
- [60] J. Kuneš, V. I. Anisimov, A. V. Lukoyanov, and D. Vollhardt, *Phys. Rev. B* **75**, 165115 (2007).
- [61] J. Q. Lin, P. Villar Arribi, G. Fabbris, A. S. Botana, D. Meyers, H. Miao, Y. Shen, D. G. Mazzone, J. Feng, S. G. Chiuzbăian, A. Nag, A. C. Walters, M. García-Fernández, K.-J. Zhou, J. Pelliciari, I. Jarrige, J. W. Freeland, J. Zhang, J. F. Mitchell, V. Bisogni, X. Liu, M. R. Norman, and M. P. M. Dean, *Phys. Rev. Lett.* **126**, 087001 (2021).
- [62] S. W. Zeng, C. J. Li, L. E. Chow, Y. Cao, Z. T. Zhang, C. S. Tang, X. M. Yin, Z. S. Lim, J. X. Hu, P. Yang, and A. Ariando, (2021), arXiv:2105.13492.
- [63] M. Osada, B. Y. Wang, B. H. Goodge, S. P. Harvey, K. Lee, D. Li, L. F. Kourkoutis, and H. Y. Hwang, (2021), arXiv:2105.13494.